arXiv:1606.07848v1 [cond-mat.str-el] 24 Jun 2016

Quantum criticality in $CeRh_{0.58}Ir_{0.42}In_5$: Kondo-breakdown and spin-density critical points

Yongkang Luo[1],* Xin Lu[2], A. P. Dioguardi[1], P. F. S. Rosa[1], E. D. Bauer[1], Qimiao Si[3], and J. D. Thompson[1]
[1] *Los Alamos National Laboratory, Los Alamos, New Mexico 87545, USA;*
[2] *Center for Correlated Matter, Zhejiang University, Hangzhou 310058, China; and*
[3] *Department of Physics and Astronomy and Center for Quantum Materials, Rice University, Houston, Texas 77005, USA.*
(Dated: June 28, 2016)

Charge and entropy transport properties of the heavy-fermion compound $CeRh_{0.58}Ir_{0.42}In_5$ were measured as a function of pressure. At atmospheric pressure, local moments in the compound order antiferromagnetically below T_N=3.5 K, and coexisting superconductivity develops below T_c^{on}=1.04 K. Applying pressure suppresses magnetic order, but a potential quantum-critical point is hidden by a dome of superconductivity. Suppressing superconductivity with an applied magnetic field, however, reveals two quantum-critical points. The in-field thermopower divided by temperature changes discontinuously at p_{c1} and reaches a symmetric peak about p_{c2}. These charge and entropy transport measurements reveal two qualitatively different quantum-critical points in $CeRh_{0.58}Ir_{0.42}In_5$: Kondo-breakdown quantum criticality at p_{c1} that involves an abrupt reconstruction of Fermi surface is followed by a spin-density critical point at p_{c2} across which the Fermi surface evolves smoothly. Such a sequence of critical points is anticipated by theoretical predictions for a "global" phase diagram of heavy-fermion materials.

PACS numbers: 75.20.Hr, 74.70.Tx, 74.62.Fj, 74.25.fg

There has been accumulating evidence for unconventional quantum-critical points (QCPs) in heavy-fermion compounds[1–8]. Generically, a QCP is an end point at absolute zero temperature of a continuous transition that separates ordered and disordered phases and is accessed by a non-thermal control parameter g, such as chemical doping (x), pressure (p) and magnetic field (B)[9]. Conventional theories of a magnetic QCP, which consider only fluctuations of an order parameter, predict a T=0 spin-density wave (SDW) transition in which the Fermi volume evolves smoothly across the QCP[10, 11]. Alternative models of unconventional criticality, frequently called local, selective Mott or Kondo-breakdown theories, invoke criticality of electronic degrees of freedom that may be coincident with magnetic criticality[12–15], and the QCP is accompanied by a sharp reconstruction of the Fermi surface (FS). It is worth noting that multiple types of QCPs can be found in the same material when those QCPs are accessed with different control parameters[8, 16, 17]. One representative example is $CeCu_{6-x}Au_x$, in which Au-doping induces local-moment-like antiferromagnetism for x>0.1 and non-SDW criticality as a function of x, yet its field-induced critical behavior is characteristic of a more conventional SDW QCP[16].

$CeRhIn_5$ is another example of a system that hosts multiple QCPs as a function of different tuning parameters. Its small Fermi volume[18] and large ordered moment below its Néel temperature T_N=3.8 K[19, 20] are consistent with Ce's $4f$ electrons being localized. Applying pressure to $CeRhIn_5$ induces superconductivity (SC) and a zero-temperature magnetic/non-magnetic transition at a critical pressure P_2=2.35 GPa[21–23], where de Haas-van Alphen (dHvA) measurements find an abrupt change from small-to-large Fermi surfaces and strong enhancement of the quasiparticle effective mass[24], characteristic of an unconventional QCP. In the absence of an applied magnetic field, these responses are hidden by a dome of SC that also encompasses a range of lower pressures where antiferromagnetic (AFM) order and SC coexist. At atmospheric pressure but as a function of magnetic field, there are two field-induced QCPs, one near 30 T where there is a change from small-to-large Fermi surface within an AFM phase[17, 25] and a SDW QCP near 50 T[17].

The evolution of magnetism and SC in the homologous series $CeRh_{1-x}Ir_xIn_5$ as a function of Ir content x is somewhat similar to $CeRhIn_5$ under pressure. For x<0.3, there is only incommensurate AFM order at $\mathbf{Q}$ = (0.5, 0.5, ∼0.297)[20], and for 0.3<x<0.6, an additional small-moment, commensurate AFM order develops and coexists with SC[26]. At higher Ir concentrations, there is only SC[27, 28]. Interestingly, as in $CeRhIn_5$ under pressure[29], the appearance of SC in $CeRh_{1-x}Ir_xIn_5$ coincides with a change of magnetic structure[26], making the similarity between these two cases even stronger. dHvA measurements show that the cyclotron frequencies are larger in $CeIrIn_5$ than in $CeRhIn_5$[18], which implies that the $4f$ electron participates in making the larger FSs of $CeIrIn_5$. Somewhere in the $CeRh_{1-x}Ir_xIn_5$ series, there should be a change in $4f$-electron localization and a magnetic QCP. Unfortunately, dHvA measurements have not been possible across the series. To explore these issues, we have measured the effect of pressure on the resistivity and thermopower of a crystal $CeRh_{0.58}Ir_{0.42}In_5$ whose composition places it close to the critical Ir concentration x_c≃0.6[27] where a magnetic boundary drops rapidly to T=0 at atmospheric pressure[26].

Single crystalline $CeRh_{0.58}Ir_{0.42}In_5$ was grown from an Indium-rich flux[27]. The Ir concentration was determined by ^{115}In nuclear quadrupole resonance (NQR)[30] and energy dispersive x-ray spectroscopy (EDX), both of which gave x=0.42(3), and EDX showed that the Ir concentration was highly uniform. Thermopower measurements were carried out by means of a steady-state technique[31]. Both electrical and thermal currents were applied along the **a**-axis that is also the direction of the external magnetic field. A hybrid piston-clamp type cell, with Daphne 7373 as the pressure medium, generated hydrostatic pressures to 2.20 GPa.

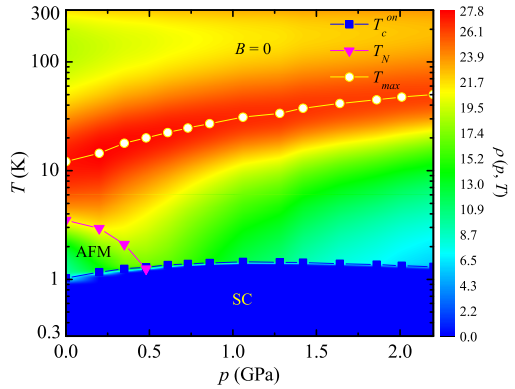

FIG. 1. A contour plot constructed from $\rho(p,T)$ at zero magnetic field (see Fig. S1 in Ref. [32]). Symbols show the evolution of resistivity maximum T_{max}, Néel temperature T_N and superconducting onset temperature T_c^{on}.

The zero-field pressure-temperature phase diagram, constructed from resistivity measurements (Fig. S1 in Ref. [32]), is summarized in Fig. 1 where we see that evidence for magnetic order disappears near 0.48 GPa below a dome of SC. A field of 9 T has a negligible effect on the Néel temperature and the temperature dependence of resistivity (inset to Fig. S1(a) in Ref. [32]), but it completely suppresses SC. In this field, however, a resistive signature for an AFM transition continues to pressures p>0.48 GPa [Fig. 2(a)]. This evolution is seen more clearly in $d\rho/dT$ that is plotted in Fig. 2(b). At ambient pressure, $d\rho/dT$ peaks near 2.5 K, which is much lower than the Néel temperature. From magnetic neutron diffraction on a sample with Ir content near x=0.42, incommensurate antiferromagnetism develops at 3.5 K and coexisting small-moment, commensurate AFM appears below 2.7 K[26]. Specific heat measurements on our crystal [inset to Fig. 2(b)] find an inflection point in C/T at 3.5 K and a peak near 2.5 K, mimicking the features in $d\rho/dT$. We, therefore, identify the inflection temperature in $d\rho/dT$ with the onset of incommensurate AFM and the peak as an approximation to the appearance of commensurate order. It is obvious from inspection of the $d\rho/dT$ curves that they narrow quickly with increasing pressure and that for 0.61≤p<1.06 GPa the peak position changes much more slowly. At 1.06 GPa, $d\rho/dT$ approaches a constant at low temperatures, signaling that $\rho(T)$ at this pressure is almost a linear function of temperature, and a well-defined signature for an AFM transition has disappeared. This is seen more clearly in the inset to Fig. 2(a) where $\rho(T)$ at 1.06 GPa is essentially T-linear below about 0.75 K and there is no detectable evidence for an AFM transition.

Further evidence for criticality comes from fitting the resistivity $\rho(T)$ to a power law:

$$\rho(T) = \rho_0 + \Delta\rho = \rho_0 + AT^n, \tag{1}$$

where ρ_0 is the residual resistivity. As also shown in the inset to Fig. 2(a), the low-temperature resistivity at 2.20 GPa follows a quadratic temperature dependence below about 1 K and is typical of a Fermi liquid. We take this pressure as a reference for normalizing lower pressure data in the false-color contour plot in Fig. 2(c). In the low temperature limit, this plot shows that the residual resistivity peaks near 0.6 GPa, and this is characteristic of strong scattering by quantum fluctuations. In this figure, solid triangles denote the temperature from Fig. 2(b) where incommensurate AFM develops. The coincidence of strongest scattering and an extrapolation of the Néel temperature of incommensurate order to T=0 suggests that there is a quantum-phase transition of this order near p_{c1} = 0.6 GPa. This conclusion is supported further by the pressure-induced collapse of the broad maximum in $d\rho/dT$ to a much narrower peak at 0.61 GPa. Nevertheless, the narrow peak persists to 1.06 GPa, indicating that another magnetic transition remains to this higher pressure. As we will demonstrate, magnetic order in this pressure range is a SDW, but neutron diffraction or NQR experiments are needed to determine the detailed nature of this order. Irrespective of the precise nature of the magnetism, the important point is that it exists in this pressure range and we label this magnetic transition T_m. Figure 2(d) presents a contour plot of the local exponent n as a function of p and T. Here, n is derived from the local derivative, n=$d(\ln\Delta\rho)/d(\ln T)$. Though the residual resistivity is a maximum near 0.6 GPa, there is only a limited temperature range above this pressure where the resistivity exhibits non-Fermi-liquid (NFL) behavior with n∼1.0. This may be due to the presence of magnetism below T_m. In contrast, residual scattering is not so enhanced and there is an extended temperature range with n∼1.0 around p_{c2}=1.06 GPa where T_c^{on} in zero field is a maximum. The apparent dichotomy of signatures for quantum criticality at p_{c1} and p_{c2} is a first indication that these QCPs may be different in character, and this is clarified through thermopower measurements.

The thermopower is given by[33]

$$S \equiv \frac{\alpha}{\sigma} = \frac{\pi^2}{3}\frac{k_B^2 T}{q}\frac{\partial \ln\sigma(\varepsilon)}{\partial\varepsilon}\bigg|_{\varepsilon=\varepsilon_F}, \tag{2}$$

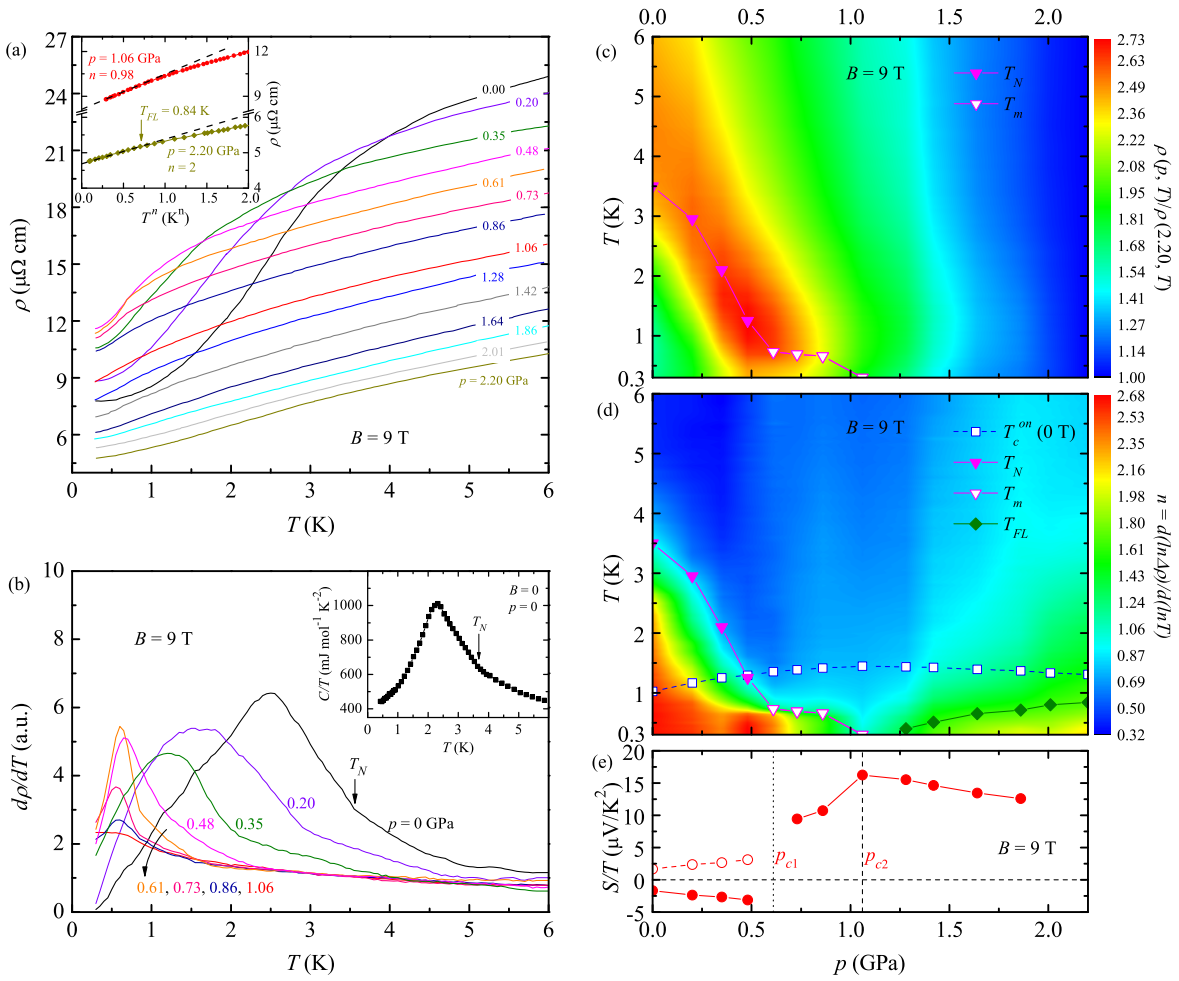

FIG. 2. Transport properties of $CeRh_{0.58}Ir_{0.42}In_5$ at B=9 T, $\mathbf{B}\|\mathbf{a}$. (a) $\rho(T)$ profiles at various pressures (data vertically shifted). The inset shows evidence for NFL and FL behaviors for p=1.06 GPa and 2.20 GPa, respectively. (b) $d\rho/dT$ for small applied pressures. The $\rho(T)$ data have been interpolated and three-point smoothed before differentiation. The inset shows temperature-dependent specific heat measured at B=0 and p=0. A weak SC anomaly can be seen in zoom-in (not shown). (c) Contour plot of isothermal resistivity normalized by the resistivity at 2.2 GPa, $\rho(p,T)/\rho(2.20,T)$. (d) Contour plot of the local exponent n=$d\ln(\Delta\rho)/d\ln(T)$ defined in Eq. (1). (e) The initial slope of thermopower, S/T, as a function of p; the open squares denote the absolute values for p<0.6 GPa.

where k_B is Boltzman's constant, q is the charge of carriers, σ is the electrical conductivity, α is the Peltier conductivity, and ε_F is the chemical potential at T=0. Being the energy-derivative of $\ln\sigma$, S is more sensitive to the Fermi-surface topology than σ. Moreover, because the entropy current $\mathbf{J}_S$=$\frac{1}{T}\boldsymbol{\alpha}\cdot\mathbf{E}$ ($\mathbf{E}$ is electric field)[34], thermopower provides a measure of transport entropy per each conduction carrier.

Figure 3(a) displays the temperature dependence of thermopower at selected pressures without an external magnetic field. Below T_c^{on}, $S(T)$ drops to 0, demonstrating an entropy-less SC ground state. S changes sign from negative to positive near 2.6 K at p=0. With applied pressure, the temperature where the sign change occurs moves to lower temperatures, and at p=0.35 GPa, it coincides with T_c^{on}. Application of a 9-T field allows tracking the sign changes to lower temperatures, as shown in Fig. 3(b). At p=0.61 GPa, $S(T)$ remains positive down to 0.3 K, the base temperature of our measurements, but may become negative at even lower temperature. A smooth extrapolation of $S(T)$ suggests that $S(T)$ remains positive to T=0 when $p\geq$0.73 GPa. The initial slope of $S(T)$ at our lowest temperatures is plotted in Fig. 2(e) as a function of p. There are two notable features: a discontinuous jump in S/T near p_{c1} and a maximum at p_{c2}. With S being sensitive to Fermi-surface topology, the jump in S/T implies a qualitative change in electronic properties at p_{c1}.

The temperature dependence of S/T around p_{c1} and p_{c2} is displayed in Figs. 3(c) and (d). For p<p_{c1}, *e.g.*

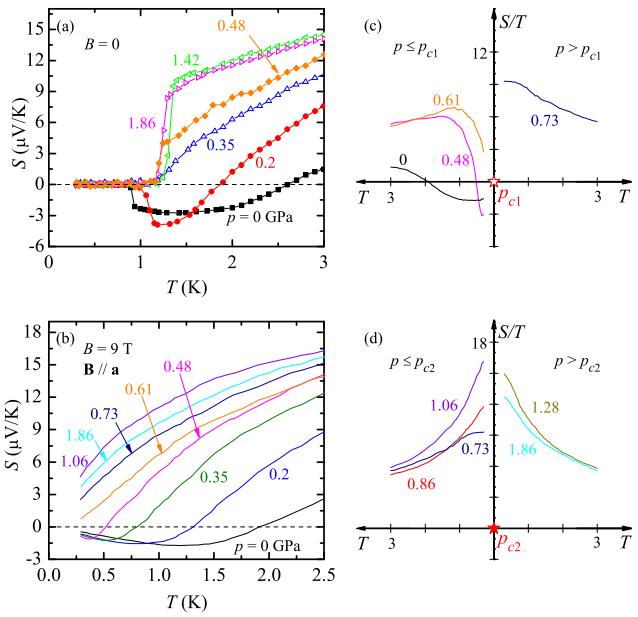

FIG. 3. Temperature dependence of thermopower under various pressures, measured at zero magnetic field (a) and 9 T (b). (c) and (d) show the temperature dependence of S/T (B=9 T) around p_{c1} and p_{c2}, respectively.

0.48 GPa, S/T initially increases with decreasing T and forms a broad peak before dropping sharply as $T\rightarrow 0$. The maximum and sharp drop in S/T move to lower temperatures for p=0.61 GPa, but at a slightly higher pressure (0.73 GPa), S/T increases monotonically with decreasing temperature and tends to saturate to a finite value as T approaches 0. In contrast to the asymmetry in S/T around p_{c1}, S/T approaches T=0 symmetrically about p_{c2} and tends to diverge in the limit of zero temperature, though it may roll over to a constant at temperatures below 0.3 K. Because S/T is proportional to the Sommerfeld coefficient of specific heat γ[35], the temperature evolution of S/T around p_{c2} is a clear signature of quantum criticality.

Models of Kondo-breakdown and SDW QCPs anticipate the behaviors we find around p_{c1} and p_{c2}[36]. Theory predicts a strong increase in S/T as T goes to zero and that this increase is symmetric about a SDW QCP as it is approached from AFM and paramagnetic states, just as we find at p_{c2}. We, therefore, identify the magnetic order below T_m as being a SDW. At a Kondo-breakdown QCP, however, S/T should be asymmetric about the QCP, in detailed agreement with experimental results at p_{c1}. In this theory[36, 37], a sharp peak in S/T on the AFM side of a Kondo-breakdown QCP is expected and signals FS reconstruction. Though the maximum in S/T at 0.61 GPa is not as sharp as predicted theoretically, some rounding of the theoretically sharp feature could be due to impurity scattering, not considered in the model, but present in $CeRh_{0.58}Ir_{0.42}In_5$. Nevertheless, agreement between experiment and theory at both p_{c1} and p_{c2} is striking [Fig. S2 in Ref. [32]] and strong evidence that the two critical points are qualitatively different in nature, p_{c1} being a Kondo-breakdown QCP and p_{c2} a SDW QCP.

A global theory of local quantum criticality, which also is based on a breakdown of the Kondo effect at a QCP, predicts a sequence of two zero-temperature phase boundaries as a function of some non-thermal tuning parameter[38, 39], which in our case is pressure. As a function of the tuning parameter, there is a T=0 boundary between a magnetically ordered state with small FS and a SDW state with large Fermi surface. As the tuning parameter is increased, this QCP is followed by another T=0 boundary between SDW and paramagnetic states. This sequence of quantum-phase transitions is realized in $CeRh_{0.58}Ir_{0.42}In_5$. Indeed, a more general view of our key conclusion is that the isothermal S/T, in the low temperature limit, undergoes a sudden negative-to-positive jump across p_{c1} [Figs. 2(e) and 3(c)]. This is consistent with a sudden change of the FS from small to large across an unconventional QCP of the Kondo-breakdown type at p_{c1}. We note that S at low temperature is negative in $CeRhIn_5$ (data not shown) but positive in $CeIrIn_5$[31]. This change in sign reflects their different electronic structures: the former consists of three electron FS sheets ($\alpha_{1,2,3}$, band-15) and one hole FS sheet (β_2, band-14)[24], but the latter has an additional hole FS sheet (β_1, band-14)[40] as well as larger overall FS.

From the magnetic phase boundaries in Fig. 2(d), we also conclude that the FS reconstruction is accompanied by a T=0 boundary between incommensurate antiferromagnetism and a SDW, as it is in $CeRhIn_5$ at very high magnetic fields[17]. If only part of the FS reconstructs at p_{c1}, it is possible that the SDW manifested at pressures between p_{c1} and p_{c2} is the small-moment, commensurate AFM order at atmospheric pressure, but if the change in electronic structure is more severe, the SDW at high pressures could have a different symmetry. Without the possibility of dHvA measurements on $CeRh_{0.58}Ir_{0.42}In_5$, determining the symmetry of the SDW at $p_{c1}\leq p\leq p_{c2}$ would provide insight on how the Fermi surface changes at p_{c1}.

In summary, pressure-dependent resistivity and thermopower measurements of heavy-fermion $CeRh_{0.58}Ir_{0.42}In_5$ reveal two quantum-critical points. There is a Kondo-breakdown critical point at p_{c1}=0.6 GPa where the Fermi surface suddenly reconstructs and there is a transition from local-moment, incommensurate antiferromagnetism to SDW order. This QCP is followed at higher pressures by a spin-density QCP at p_{c2}=1.06 GPa. Thermopower measurements around these critical points are a particularly clear experimental manifestation of theoretical predictions. Further, the sequence of QCPs and their natures are anticipated in the global phase diagram of local quantum criticality that also requires critical destruction of the Kondo effect.

It seems likely that the criticality in $CeRh_{0.58}Ir_{0.42}In_5$ generalizes to other members in this series and underlies their superconductivity.

We thank T. Park, F. Ronning, J. Lawrence and H. Löhneysen for insightful conversations and J. L. Sarrao for providing the sample used in this study. Work at Los Alamos was performed under the auspices of the U.S. Department of Energy, Division of Materials Sciences and Engineering. A. Dioguardi and P. F. S. Rosa acknowledge Director's Postdoctoral Fellowships supported through the Los Alamos LDRD program. Work at Rice University was in part supported by NSF and the Robert A. Welch Foundation Grant No. C-1411.

* ykluo@lanl.gov

[1] A. Schröder, G. Aeppli, R. Coldea, M. Adams, O. Stockert, H. v. Löhneysen, E. Bucher, R. Ramazashvili, and P. Coleman, Nature **407**, 351 (2000).
[2] J. Custers, P. Gegenwart, H. Wilhelm, K. Neumaier, Y. Tokiwa, O. Trovarelli, C. Geibel, F. Steglich, C. Pepin, and P. Coleman, Nature **424**, 524 (2003).
[3] S. Friedemann, T. Westerkamp, M. Brando, N. Oeschler, S. Wirth, P. Gegenwart, C. Krellner, C. Geibel, and F. Steglich, Nat. Phys. **5**, 465 (2009).
[4] J. Arndt, O. Stockert, K. Schmalzl, E. Faulhaber, H. S. Jeevan, C. Geibel, W. Schmidt, M. Loewenhaupt, and F. Steglich, Phys. Rev. Lett. **106**, 246401 (2011).
[5] J. Custers, K.-A. Lorenzer, M. Müller, A. Prokofiev, A. Sidorenko, H. Winkler, A. M. Strydom, Y. Shimura, T. Sakakibara, R. Yu, Q. Si, and S. Paschen, Nat. Mater. **11**, 189 (2012).
[6] S. Paschen, T. Luhmann, S. Wirth, P. Gegenwart, O. Trovarelli, C. Geibel, F. Steglich, P. Coleman, and Q. Si, Nature **432**, 881 (2012).
[7] Y. Luo, L. Pourovskii, S. E. Rowley, Y. Li, C. Feng, A. Georges, J. Dai, G. Cao, Z. Xu, Q. Si, and N. P. Ong, Nat. Mater. **11**, 777 (2014).
[8] Y. Luo, F. Ronning, N. Wakeham, X. Lu, T. Park, Z. A. Xu, and J. D. Thompson, Proc. Natl. Acad. Sci. USA **112**, 13520 (2015).
[9] H. v. Löhneysen, A. Rosch, M. Vojta, and P. Wölfle, Rev. Mod. Phys. **79**, 1015 (2007).
[10] J. A. Hertz, Phys. Rev. B **14**, 1165 (1976).
[11] A. J. Millis, Phys. Rev. B **48**, 7183 (1993).
[12] Q. Si, S. Rabello, K. Ingersent, and J. L. Smith, Nature **413**, 804 (2001).
[13] P. Coleman and A. J. Schofield, Nature **433**, 226 (2005).
[14] P. Gegenwart, Q. Si, and F. Steglich, Nature Phys. **4**, 186 (2008).
[15] C. Pépin, Phys. Rev. B **77**, 245129 (2008).
[16] H. v. Löhneysen, C. Pfleiderer, T. Pietrus, O. Stockert, and B. Will, Phys. Rev. B **63**, 134411 (2001).
[17] L. Jiao, Y. Chen, Y. Kohama, D. Graf, E. D. Bauer, J. Singleton, J.-X. Zhu, Z. Weng, G. Pang, T. Shang, J. Zhang, H.-O. Lee, T. Park, M. Jaime, J. D. Thompson, F. Steglich, Q. Si, and H. Q. Yuan, Proc. Natl. Acad. Sci. USA **112**, 673 (2015).
[18] H. Shishido, R. Settai, D. Aoki, S. Ikeda, H. Nakawaki, N. Nakamura, T. Iizuka, Y. Inada, K. Sugiyama, T. Takeuchi, K. Kindo, T. Kobayashi, Y. Haga, H. Harima, Y. Aoki, T. Namiki, H. Sato, and Y. Ōnuki, J. Phys. Soc. Jpn. **71**, 162 (2002).
[19] H. Hegger, C. Petrovic, E. G. Moshopoulou, M. F. Hundley, J. L. Sarrao, Z. Fisk, and J. D. Thompson, Phys. Rev. Lett. **84**, 4986 (2000).
[20] W. Bao, P. G. Pagliuso, J. L. Sarrao, J. D. Thompson, Z. Fisk, J. W. Lynn, and R. W. Erwin, Phys. Rev. B **62**, R14621 (2000).
[21] G. Knebel, D. Aoki, D. Braithwaite, B. Salce, and J. Flouquet, Phys. Rev. B **74**, 020501 (2006).
[22] T. Park, F. Ronning, H. Q. Yuan, M. B. Salamon, R. Movshovich, J. L. Sarrao, and J. D. Thompson, Nature **440**, 65 (2006).
[23] T. Park and J. D. Thompson, New J. Phys. **11**, 055062 (2009).
[24] H. Shishido, R. Settai, H. Harima, and Y. Ōnuki, J. Phys. Soc. Jpn. **74**, 1103 (2005).
[25] P. J. W. Moll, B. Zeng, L. Balicas, S. Galeski, F. F. Balakirev, E. D. Bauer, and F. Ronning, Nat. Commun. **6**, 6663 (2016).
[26] A. Llobet, A. D. Christianson, W. Bao, J. S. Gardner, I. P. Swainson, J. W. Lynn, J.-M. Mignot, K. Prokes, P. G. Pagliuso, N. O. Moreno, J. L. Sarrao, J. D. Thompson, and A. H. Lacerda, Phys. Rev. Lett. **95**, 217002 (2005).
[27] P. G. Pagliuso, C. Petrovic, R. Movshovich, D. Hall, M. F. Hundley, J. L. Sarrao, J. D. Thompson, and Z. Fisk, Phys. Rev. B **64**, 100503 (2001).
[28] M. Nicklas, V. A. Sidorov, H. A. Borges, P. G. Pagliuso, J. L. Sarrao, and J. D. Thompson, Phys. Rev. B **70**, 020505 (2004).
[29] N. Aso, K. Ishii, H. Yoshizawa, T. Fujiwara, Y. Uwatoko, G.-F. Chen, N. K. Sato, and K. Miyake, J. Phys. Soc. Jpn. **78**, 073703 (2009).
[30] G.-q. Zheng, N. Yamaguchi, H. Kan, Y. Kitaoka, J. L. Sarrao, P. G. Pagliuso, N. O. Moreno, and J. D. Thompson, Phys. Rev. B **70**, 014511 (2004).
[31] Y. Luo, P. F. S. Rosa, E. D. Bauer, and J. D. Thompson, Phys. Rev. B **93**, 201102 (2016).
[32] See Supplemental Material at ****** for additional resistivity and S/T details.
[33] J. M. Ziman, *Principles of the Theory of Solids* (Cambridge University Press, Cambridge, 1972).
[34] R. T. Delves, Rep. Prog. Phys. **28**, 249 (1965).
[35] K. Behnia, D. Jaccard, and J. Flouquet, J. Phys.: Condens. Matter **16**, 5187 (2004).
[36] K.-S. Kim and C. Pépin, Phys. Rev. B **81**, 205108 (2010).
[37] K.-S. Kim and C. Pépin, Phys. Rev. B **83**, 073104 (2011).
[38] Q. Si, Physica B **378-380**, 23 (2006).
[39] E. M. Nica, K. Ingersent, and Q. Si, arXiv: 1603.03829 (2016).
[40] Y. Haga, Y. Inada, H. Harima, K. Oikawa, M. Murakawa, H. Nakawaki, Y. Tokiwa, D. Aoki, H. Shishido, S. Ikeda, N. Watanabe, and Y. Ōnuki, Phys. Rev. B **63**, 060503 (2001).

Supplemental Material:

Quantum criticality in $CeRh_{0.58}Ir_{0.42}In_5$: Kondo-breakdown and spin-density critical points

Yongkang Luo[1*], Xin Lu[2], A. P. Dioguardi[1], P. F. S. Rosa[1], E. D. Bauer[1], Qimiao Si[3], and J. D. Thompson[1]
[1] *Los Alamos National Laboratory, Los Alamos, New Mexico 87545, USA;*
[2] *Center for Correlated Matter, Zhejiang University, Hangzhou 310058, China; and*
[3] *Department of Physics and Astronomy and Center for Quantum Materials, Rice University, Houston, Texas 77005, USA.*

In this ***Supplemental Material (SM)***, we provide additional resistivity data, and a comparison of experimental S/T to model calculations that further support the discussion and conclusions of the main text.

SM I: Pressure dependent $\rho(T)$ at B=0

Figure S1 shows the temperature dependence of resistivity of $CeRh_{0.58}Ir_{0.42}In_5$ at pressures to 2.20 GPa. At ambient pressure, $\rho(T)$ initially decreases upon cooling but starts to increase below 135 K and forms a pronounced broad peak around T_{max}=12 K, characteristic of the onset of coherent Kondo scattering. Below T_{max}, $\rho(T)$ decreases monotonically, and the sample becomes a superconductor with an onset critical temperature T_c^{on}=1.04 K. Above T_c^{on}, another feature near T_N=3.5 K reflects a reduction of spin-scattering due to the formation of long range AFM order of Ce moments[1–4]. Under pressure, (i) T_{max} increases monotonically and reaches ∼50 K at 2.20 GPa; (ii) T_c^{on} increases with pressure and reaches a maximum of 1.45 K at p=1.06 GPa before it starts to decrease [Fig. S1(b)]; and, (iii) the AFM order is gradually suppressed and becomes unresolvable when p>0.48 GPa where the resistive anomaly is concealed by SC. A field of 9 T (**B**‖**a**) completely suppresses SC, but has a negligible effect on the temperature dependence of the resistivity and the AFM signature, as seen from the inset to Fig. S1(a).

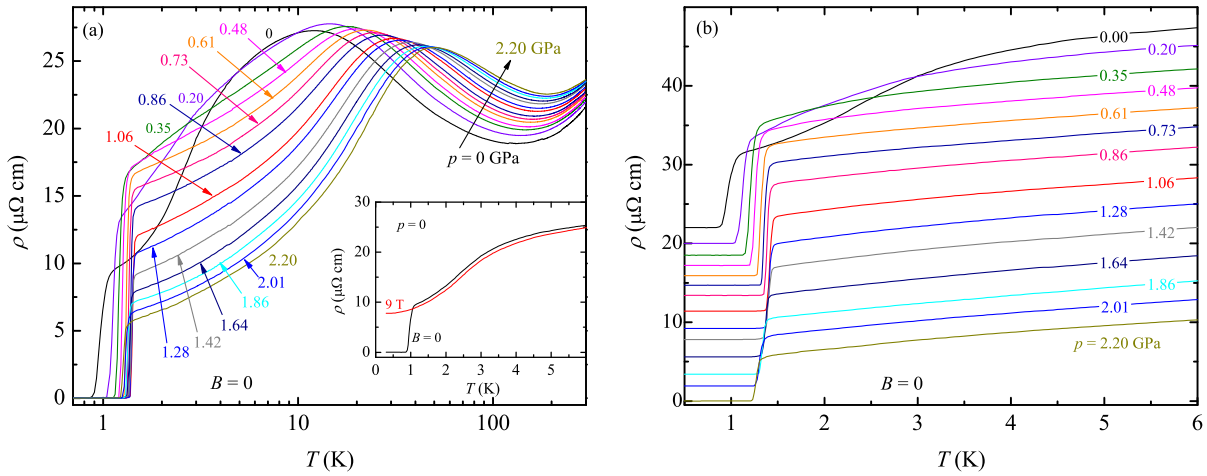

FIG. S1. (a) Temperature-dependent resistivity of $CeRh_{0.58}Ir_{0.42}In_5$ under different pressures. The inset is a comparison of $\rho(T)$ for B=0 and 9 T at ambient pressure. (b) shows a zoom-in view of the low temperature region, and the curves have been vertically shifted for clarity.

SM II: S/T at QCPs - experimental and theoretical

Thermopower has been predicted theoretically as a fingerprint of quantum criticality in heavy-fermion materials[5, 6]. For a Kondo-breakdown QCP, theory predicts Fermi-surface reconstruction on a small energy scale E^* on the localized side of a QCP [g<g_c in Fig. S2(c)]. This reconstruction produces an abrupt discontinuity in S/T at the QCP, and depending on details of a particular material, there may be a sign change in S/T. In contrast, for a SDW

QCP, because a large Fermi surface varies smoothly across the QCP, S/T is symmetric and saturates. A comparison of S/T behaviors between experimental results (this work) and theoretical prediction is shown in Fig. S2.

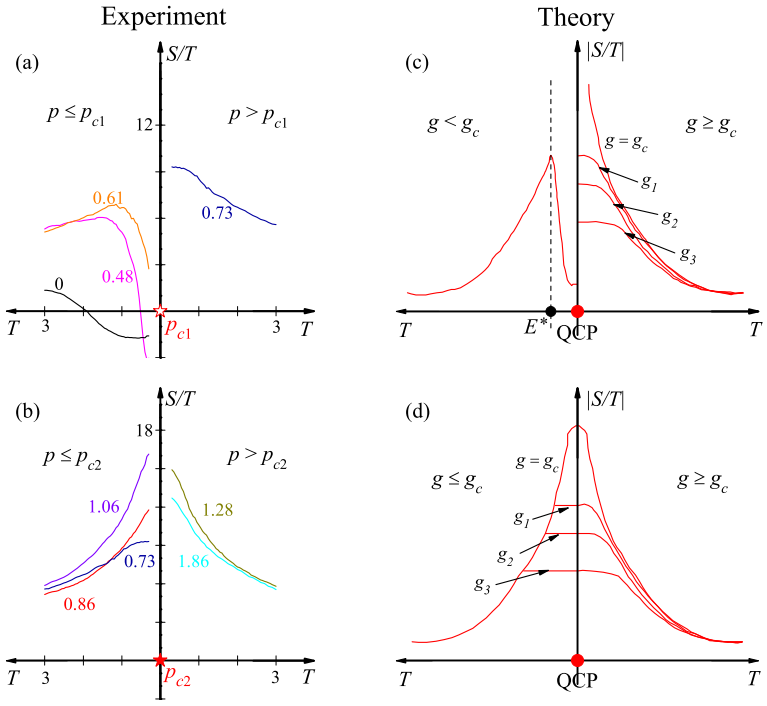

FIG. S2. A comparison of S/T behaviors about a Kondo-breakdown QCP (upper panels) and a SDW QCP (lower panels). The left column shows experimental data (this work), and the right column shows the theoretical predictions reproduced from Ref. [5]. A QCP appears at a critical value of a tuning parameter g_c. Values of g_1, g_2 and g_3 tune the system progressively away from a QCP. Note that theoretical curves are absolute values of S/T.

* ykluo@lanl.gov

[1] A. Llobet, A. D. Christianson, W. Bao, J. S. Gardner, I. P. Swainson, J. W. Lynn, J.-M. Mignot, K. Prokes, P. G. Pagliuso, N. O. Moreno, J. L. Sarrao, J. D. Thompson, and A. H. Lacerda, Phys. Rev. Lett. **95**, 217002 (2005).
[2] P. G. Pagliuso, C. Petrovic, R. Movshovich, D. Hall, M. F. Hundley, J. L. Sarrao, J. D. Thompson, and Z. Fisk, Phys. Rev. B **64**, 100503 (2001).
[3] M. Nicklas, V. A. Sidorov, H. A. Borges, P. G. Pagliuso, J. L. Sarrao, and J. D. Thompson, Phys. Rev. B **70**, 020505 (2004).
[4] G.-q. Zheng, N. Yamaguchi, H. Kan, Y. Kitaoka, J. L. Sarrao, P. G. Pagliuso, N. O. Moreno, and J. D. Thompson, Phys. Rev. B **70**, 014511 (2004).
[5] K.-S. Kim and C. Pépin, Phys. Rev. B **81**, 205108 (2010).
[6] K.-S. Kim and C. Pépin, Phys. Rev. B **83**, 073104 (2011).